ARTICLE

DOI: 10.1590/2317-4889201920190028

BJGEO Brazilian Journal of Geology

The role of airborne geophysics in the investigation of gold occurrences in the Itapetim Region, Borborema Province, Northeast Brazil

Laís Cristina Leite Pereira[1]*, Lauro Cézar Montefalco de Lira Santos[1], Thais Andressa Carrino[1]

Abstract

We present a combined analysis of airborne geophysical data (magnetics and gamma-ray spectrometry) and field aspects of Itapetim lode gold district region, aiming to identify structurally deformed and hydrothermally altered zones, which are suggestive of gold mineralized sectors. The main geophysical lineaments are oriented in the NE-SW and E-W directions and display a clear correlation with the major gold-bearing structures in the region. In the magnetic maps, the key pathfinder for gold occurrences is their association with strongly magnetized areas positioned along the Itapetim Shear Zone and outer contour of Teixeira Batholith. In the field, such structures are materialized in protomylonitic and mylonitic rocks that present evidence of ductile and brittle deformation, whereas kinematic criteria are suggestive of a transpressional tectonic regime. In addition, the main radiometric pattern is characterized by K enrichment, which is correlated with a hydrothermal mineral assemblage dominated by quartz, potassium feldspar, and tourmaline. Based on the obtained data integration, we produced an integrative map and located ten new target areas of possible gold mineralization, which is correlative to other well-known lode deposits in Northeast Brazil and Africa.

KEYWORDS: Airborne geophysics; lode-type gold deposits; Itapetim gold district; Borborema Province; hydrothermal alteration.

INTRODUCTION

The occurrence and concentration of gold in the continental crust requires a combination of several geological processes, including specific tectonic settings, unique structural framework, and successive episodes of rock-fluid interaction (Groves *et al.* 2003 and references therein). Orogenic-related (lode-type) deposits are established in accretionary and collisional orogenic systems, mainly in the late subduction stages, which are triggered by crustal shortening via compressional and transpressional/transcurrent regimes (Groves *et al.* 2003, 2018, Goldfarb & Groves 2015). General geological aspects of these deposits comprehend association with trans-lithospheric faults, occurrence in terranes that experienced greenschist facies metamorphism, hydrothermal alteration, and a predominant quartz, carbonate, mica, chlorite, pyrite, scheelite, and tourmaline paragenesis (McCuaig & Kerrich 1998). Large-scale ductile shear zones are considered tectonic corridors for fluid percolation and subsequent metal concentration during metamorphism of oceanic rock sequences or devolatilization of the sediment wedge above the subduction slabs (Hronsky & Groves 2008, Groves & Santosh 2015).

Borborema Province in Northeast Brazil is a complex Neoproterozoic orogenic system that has experienced several episodes of collision and accretion tectonics, resulting in a complex array of deep-seated shear zones that present continuity along major African mobile belts (Santos & Medeiros 1999, Brito Neves *et al.* 2000, Archanjo *et al.* 2008, Santos *et al.* 2017a). Important mineralization sites in the province are restricted to some domains, including the Seridó Belt (Northern Borborema Province), which hosts Be-Ta-Sn-Li-bearing pegmatites (*e.g.*, Baumgartner *et al.* 2006, Santos *et al.* 2014) and W-Mo-Au-Bi-Te in skarns lenses (*e.g.*, Souza Neto *et al.* 2008, Hollanda *et al.* 2017). On the other hand, Au-bearing lithotypes are present in the Central Borborema Province and are usually associated with large-scale shear zones (Coutinho 1994, Coutinho & Aderton 1998, Santos *et al.* 2014). Between the states of Pernambuco and Paraíba, gold mineralization is related to Itapetim gold district, which is considered the best-known example of Au mineralized quartz lodes hosted in supracrustal (*e.g.* biotite-muscovite schist and biotite gneiss) and granitic rocks of the central Borborema Province (Scheid & Ferreira 1991, Coutinho 1994, Santos *et al.* 2014). In the region, gold-bearing rocks occur discontinuously along a 25 km-long area by 0.2 km wide (Wanderley 1999) and are considered a classical example of orogenic gold deposit (Coutinho 1994, Maia 2002, Almeida 2003).

Over the last decades, airborne magnetic and gamma-ray data have been widely applied in different areas of earth sciences, such as geological mapping (*e.g.*, Dickson & Scott 1997,

[1]Departamento de Geologia, Universidade Federal de Pernambuco – Recife (PE), Brazil. E-mails: leite_lais@hotmail.com, lauromontefalco@gmail.com, thais.carrino@gmail.com

*Corresponding author.

Madrucci *et al.* 2003, Metelka *et al.* 2011) and tectonic studies (*e.g.*, Patra *et al.* 2016, Oskooi & Abedi 2015, Santos *et al.* 2017b). Regarding exploration targets, they have been successfully applied in the study of gold deposits associated with major structures and/or hydrothermally altered areas over the globe (*e.g.*, Shives *et al.* 2000, Airo 2002, Airo & Mertanen 2008, Holden *et al.* 2012, Ramos *et al.* 2014, Wemegah *et al.* 2015, Bedini & Rasmussen 2018).

In general, the geological characteristics of Itapetim region (*i.e.*, association of Au mineralization with shear zones and granitic bodies) are favorable to the use of airborne geophysics as a tool to provide better geological and structural background to this important economic district. In this paper, we aim to determine the main general and local structural frameworks of the area using airborne magnetics and to analyze the main characteristics of radiometric images, including maps of individual counts, K/eTh ratio and ternary composition. Such data are integrated mesoscopic and microscopic structural observations as an attempt to foment new information for further prospective campaigns.

GEOLOGICAL SETTING

Borborema Province is in the Northeastern portion of Brazil and represents one of the major Neoproterozoic structural provinces of South America (Almeida *et al.* 1981). It comprises basement domains formed by Paleoproterozoic gneissic and migmatitic rocks and some Archean nuclei (Dantas *et al.* 2013, Costa *et al.* 2015, Santos *et al.* 2015, 2017a, Lima *et al.* 2019) that are interleaved or partially covered by Meso- to Neoproterozoic metasedimentary and metavolcanic sequences and terranes, which are later intruded by several Ediacaran granitic plutons associated with the Brasiliano Orogeny (Van Schmus *et al.* 1995, 2008, 2011, Brito Neves *et al.* 2000, 2014, 2016, Neves *et al.* 2006, Sial & Ferreira 2016, Basto *et al.* 2019, Santos *et al.* 2018). Based on the general displacement of the major shear zones (*i.e.*, Patos and Pernambuco lineaments), the province is divided into three subprovinces: Northern, Transversal, and Southern (Santos *et al.* 2000, Brito Neves *et al.* 2000), as seen in Fig. 1A.

The development of Borborema Province has been interpreted as a result of systematic episodes of terranes accretion during the Neoproterozoic in the light of the West Gondwana Assembly (Santos 1995, Brito Neves *et al.* 2000, 2014, Santos *et al.* 2018). See Neves (2003, 2018) and Neves *et al.* (2006) for a different interpretation for the Neoproterozoic evolution of the province. During the Brasiliano orogenic cycle, several strike-slip, thrust and suture zones (Cordani *et al.* 2013, Ganade de Araújo *et al.* 2014) were developed. Part of them has been attributed as coeval with the main Neoproterozoic ore-forming events in the province, such as the Au, W-Mo and W-Mo-Au deposits in the Northern Subprovince (Luiz-Silva *et al.* 2000, Araújo *et al.* 2005, Souza Neto *et al.* 2008, Santos *et al.* 2014, Hollanda *et al.* 2017) and Au and sulfide occurrences in the Central Subprovince (Coutinho 1994, Coutinho & Alderton 1998).

The Central Subprovince covers São José do Caiano, Piancó-Alto Brigída, Alto Pajeú, Alto Moxotó and Rio Capibaribe terranes, which are limited by regional shear zones. The studied area is in the northern boundary of Alto Pajeú Terrane, and its lithostratigraphic framework consists of Meso- to early Neoproterozoic gneissic- migmatitic and metavolcanossedimentary complexes that are intruded by late Neoproterozoic granitic suites (Bittar 1998, Santos 1996, Ferreira & Santos 2000, Medeiros 2004, Fig. 1B). The most important unit of this terrane is the *ca.* 856 Ma São Caetano Complex, which is composed by pelitic metasedimentary (muscovite-biotite gneiss with garnet, muscovite schist, marble) and meta-volcanoclastic rocks. Riacho Gravatá Complex (*ca.* 920 Ma) is another important metavolcanossedimentary unit, constituted by basic to acidic metavolcanic rocks, metapelites, and metapsamites. Other late Mesoproterozoic to early Neoproterozoic units are Riacho do Forno and Recanto metagranitic and migmatitic rocks, whose protoliths are related to Cariris Velhos orogeny (*ca.* 1000–920 Ma; Santos *et al.* 2010).

The youngest supracrustal unit of the region is Santana dos Garrotes Formation (*ca.* 730 Ma), formed by metaturbidites (biotite-muscovite schist and phyllite with sericite and chlorite) and acidic to intermediate metavolcanic rocks (Medeiros 2004). The intrusive late Neoproterozoic granitic rocks in the area have calc-alkalic, shoshonitic, and trondhjemitic affinities (Ferreira & Santos 2000, Sial & Ferreira 2016). Teixeira Batholith (*ca.* 591 Ma) represents one of the most expressive granitic pulses in the studied area. Archanjo *et al.* (2008) divided the batholith into four major regions: Mãe d'Água, Jabre, Teixeira, and São Sebastião, considering structural aspects, such as the presence of pinched, sheared, and fractured zones (Fig. 1B).

The studied area is marked by gentle to vertical dipping foliation, as well as NE-SW trending regional folds, which are related to regional scale shear zones (Medeiros 2004). For instance, the NE-SW sinistral trending Serra do Caboclo Shear Zone represents the limit of Piancó-Alto Brígida and Alto Pajeú terranes, whereas Patos Lineament marks the boundary between the Northern and Central subprovinces (Santos & Medeiros 1999, Brito Neves *et al.* 2000).

General aspects of Itapetim gold district

Early regional investigations describe the gold mineralization in Itapetim District as associated with quartz veins that occur along strongly deformed schists of São Caetano Complex and meta-granites and orthogneisses related to Neoproterozoic orogenic episodes (Coutinho 1994). These veins occasionally present a slight wall-rock alteration characterized from the inner to distal parts, by zones enriched in quartz, tourmaline and some quartz, and potassium feldspar and albite, and minor quartz and sericite (Coutinho 1994, Coutinho & Alderton 1998). This pattern is noticed in different host lithotypes (*e.g.*, schist, gneiss), which suggest that the fluid content was not affected by the chemistry of host rocks (Coutinho 1994, Coutinho & Alderton 1998).

Ferreira & Santos (2000) registered 21 gold occurrences over Itapetim gold district (Fig. 1B) and three of them exhibit

significant gold content values: Degredo, Sertãozinho, and Pimenteiras. Degredo and Sertãozinho sectors are hosted by biotite gneisses (Scheid & Ferreira 1991) and presented an average gold content, in their richest sectors, of 3 (Silva Filho 1989) and 5 g/t (CPRM 1984), respectively, whilst the Pimenteiras sector, which is hosted by biotite-muscovite schists (Scheid & Ferreira 1991), reached up to 4.1 g/t (Wanderley 1999).

The mineralized bodies show variable dimensions. Their length and width achieved, respectively, 10 to 12 m and 1.5 to 2.0 m (Wanderley 1999). In general, they present a boudin geometry concordant to the mylonitic foliation (Wanderley 1999). Sertãozinho sector is characterized by almond-shaped boudins, while Pimenteiras sector shows cylindrical boudins (pipes) disposed vertically (Silva Filho 1989).

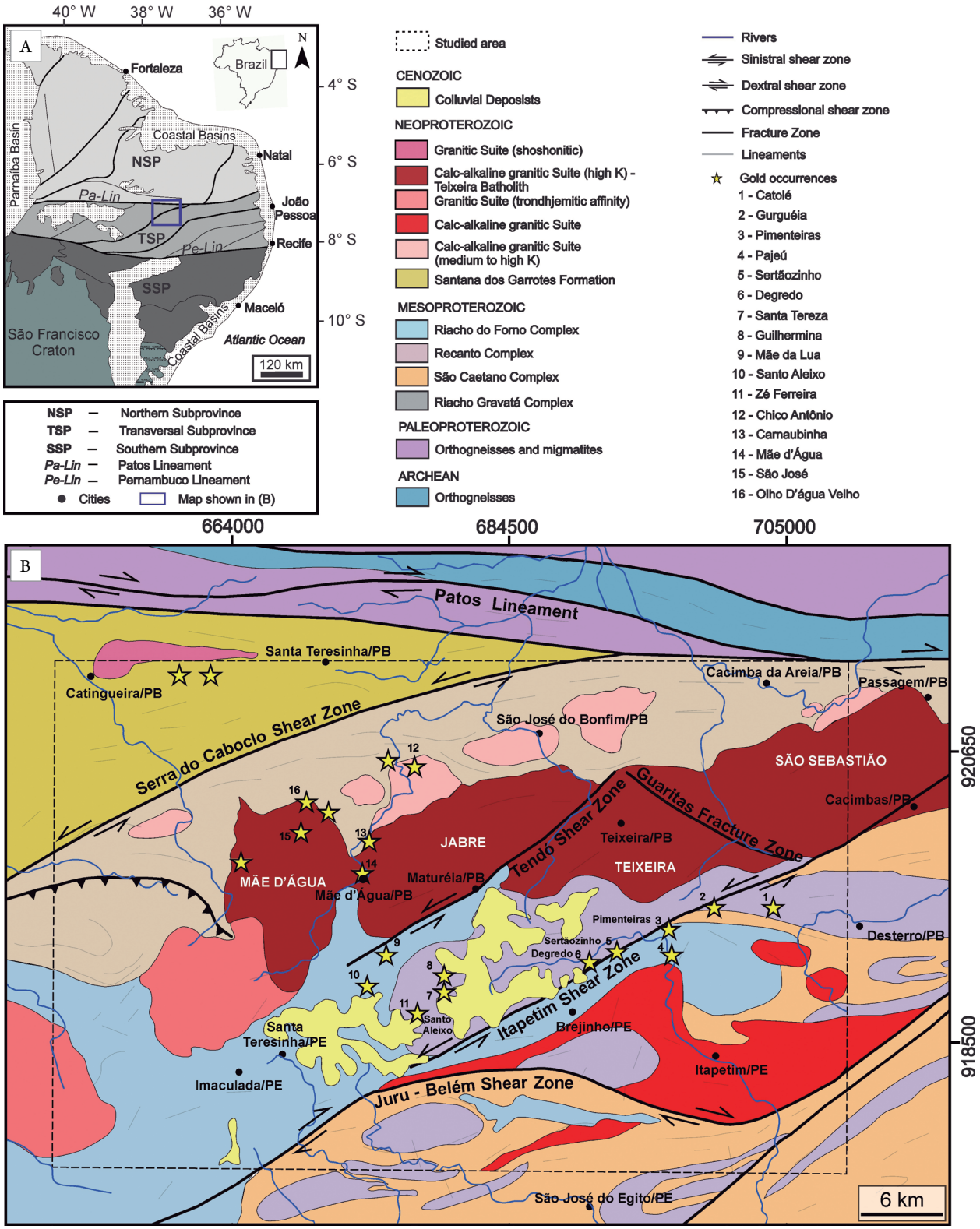

PB: State of Paraíba; PE: State of Pernambuco; P.S.: gold sectors non-referenced with numbers do not have a specific nomenclature.

Figure 1. (A) Simplified map of Borborema Province and sub-provinces (modified from Santos *et al.* 2014). (B) Geologic map of Itapetim Gold District region (modified from Ferreira & Santos 2000, Archanjo *et al.* 2008) and location of the gold occurrences.

MATERIALS AND METHODS

The geophysical data used in this study were obtained through the Pernambuco-Paraíba Airborne Geophysical Project managed by the Geological Survey of Brazil (CPRM), between 2009 and 2010 (LASA Engenharia e Prospecções S/A & PROSPECTORS Aerolevantamentos e Sistemas LTDA 2009). The flight (N-S) and tie (E-W) lines were spaced at 500 and 10,000 m, respectively. The nominal flight height was 100 m, and the interval of the measurements was 0.1 s for magnetic and 1 s for gamma-ray spectrometry. Data related to gamma-ray spectrometry (K, eTh, eU channels) and magnetics (anomalous magnetic field) were previously gridded by CPRM, using the minimum curvature and bidirectional techniques, respectively, and a cell size of 125 m.

As to magnetic data, the anomalous magnetic field and the images of the first vertical derivative (DZ) and the analytic signal amplitude (ASA) were used for visual interpretation of the structural pattern, revealing the location and major direction of shear and faults zones, as well as the anomalies associated with granitic bodies and their relations with gold occurrences. The DZ filter has been used to enhance high frequencies, in order to eliminate long-wavelength regional effects and attenuate the effects of adjacent anomalies (Milligan & Gunn 1997). In general, the ASA filter is used as an edge-detection tool (*e.g.*, Roest *et al.* 1992). However, it might have been carefully used, mainly in low latitude areas, due to its dependency on aspects as observation surface, dipping, and proximity of magnetic bodies in the area (*e.g.*, Lin-ping & Zhi-ning 1998, Li 2006).

Airborne gamma-ray spectrometry data were applied to identify the distribution and intensities of radioactive elements (K, eTh and eU) over the main lithologies through the qualitative analysis of individual channels and RGB ternary composition image of K, eTh and eU, leading to set up a litho-geophysical map. In addition, the K/eTh ratio image was also analyzed to determine where the relative concentrations of K were elevated compared with Th.

Magnetic and radiometric lineaments were qualitatively interpreted. These were divided into two categories: major, which are related to unit limits and/or shear zones, and secondary, which are associated with minor, linear/curvilinear segments. Rose diagrams made with the directions of magnetometric lineaments were also produced. All the presented maps are in UTM coordinates, placed on the WGS 84 datum and 24S zone. In field, three of the 21 gold occurrences registered in Itapetim gold district were visited (Pimenteiras, Degredo, and Santo Aleixo), and the major results obtained here about hydrothermal mineral assemblages are related to these mineralized areas. Mineral abbreviations used in field and thin section pictures follow the standard suggested by Whitney & Evans (2010).

RESULTS

Airborne magnetic data

The structural pattern of the study area is marked by a predominance of NE-SW magnetic lineaments, but E-W and NW-SE alignments occur subordinately. The length of lineaments varies from around 1 to 40 km, as observed in the magnetic anomalies image (Fig. 2). ASA and DZ images and their respective interpreted lineament maps are shown in Figure 3.

Two main types of magnetic anomalies could be distinguished: zones of strong (~ 0.100–0.259 nT/m) and weak (< 0.050 nT/m; Fig. 3A) gradients. The former is represented by linear structures occurring in the northern and southeastern portions of the area, generally showing a rough surface (high spatial frequency). The second type is more frequent in the central-south sectors and is characterized by smooth magnetic relief, showing, punctually, scattered magnetic highs. Close to Mãe d'Água, Teixeira and Itapetim cities, these zones of weak gradient have a relatively circular/ellipsoidal shape, which are outlined by strongly high gradients (Figs. 3A and 3B), whose pattern is spatially related to Teixeira Batholith. The gold occurrences registered around the batholith (about six) are associated with those magnetic highs and are concentrated in the north edge of Mãe d'Água sector.

The NE-SW Serra do Caboclo Shear Zone, indicated as a major lineament in the NW sector (Figs. 3C and 3D), shows the strongest and most continuous magnetic anomalies and it is the widest structure of the region, which is also marked as a series of secondary lineaments in its range of influence. The strong positive anomalies located in the north of the studied area (close to Santa Teresinha and Cacimba da Areia cities) coincide with mapped gold occurrences and are closely related to the crustal influence of Patos Lineament. Despite the low coverage zone, it is still possible to observe that the magnetic lineaments are oriented E-W (Figs. 3C and 3D).

The signature of NE-SW Itapetim Shear Zone is quite variable. It crosscuts the eastern part of the studied area and is characterized by medium magnetic gradients (~ 0.030–0.050 nT/m; Fig. 3A) in its boundaries and high gradients (~ 0.050–0.150 nT/m; Fig. 3A) in its central sector. The strongly magnetized region in the center of Itapetim Shear Zone (~ 25 km by 3 km; Fig. 3A) has substantial importance due to the presence of gold occurrences (about six), including three of the

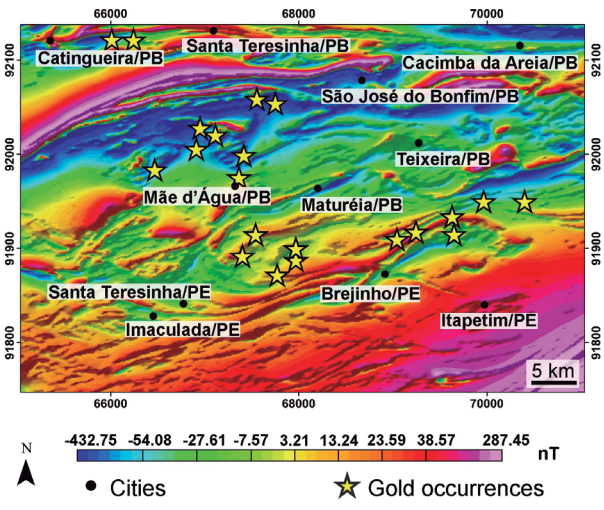

PB: State of Paraíba; PE: State of Pernambuco.

Figure 2. Magnetic anomalies of Itapetim gold district region and location of gold occurrences.

most voluminous: Sertãozinho, Pimenteiras, and Degredo (Silva Filho 1989, Wanderley 1999).

The Tendó Shear Zone is characterized as a narrow magnetic lineament that crosscuts and borders Teixeira Batholith, in the NE-SW, between Maturéia and Teixeira cities (Figs. 3A and 3B). The contour of Juru-Belém Shear Zone, unlike the other structures, was poorly defined through magnetic data. Only sparse medium to high gradients (~ 0.030–0.100 nT/m; Fig. 3A) were observed, possibly due to the low amount of magnetic minerals in its total length.

In spite of the existence of a set of three gold occurrences, associated with medium to low gradient (~ 0.010–0.020 nT/m; Fig. 3A) in the central region of the studied area, the majority of gold occurrences have in common the positioning in zones of high or extremely high gradient (~ 0.100–1.500 nT/m; Fig. 3A), and emplacement along Neoproterozoic structures, such as the Itapetim Shear Zone (ISZ) or around Teixeira Batholith.

Airborne gamma-ray spectrometric data

Radiometric maps

The potassium map is strongly representative of major granitic bodies. For instance, the extensive NE-SW segment of high K measurements (Fig. 4A, domain 1) represents Teixeira Batholith. Along this granitic domain, K concentration varies from ~ 4.40 to 10.75% in the NE portion, and from ~ 2.80 to 8.30% in the SW. The gold mineralizations associated with granites are concentrated in its SW part. Intermediate to strong K signatures (~ 3.50–8.30%; Fig. 4A, domains 2 and 3) are also verified in the central-southern region of the studied area and are closely related to the gneisses of Cariris Velhos Granitic Suite (Riacho do Forno and Recanto complexes) and other granites, as Brejinho Pluton. Nearby the ISZ, the gold occurrences are positioned in a NE-SW corridor, whose K content varies from medium to very high (~ 3.40–8.30% K). Extremely low values on K (< 1.22% K; Fig. 4A, domains 4 and 5) are

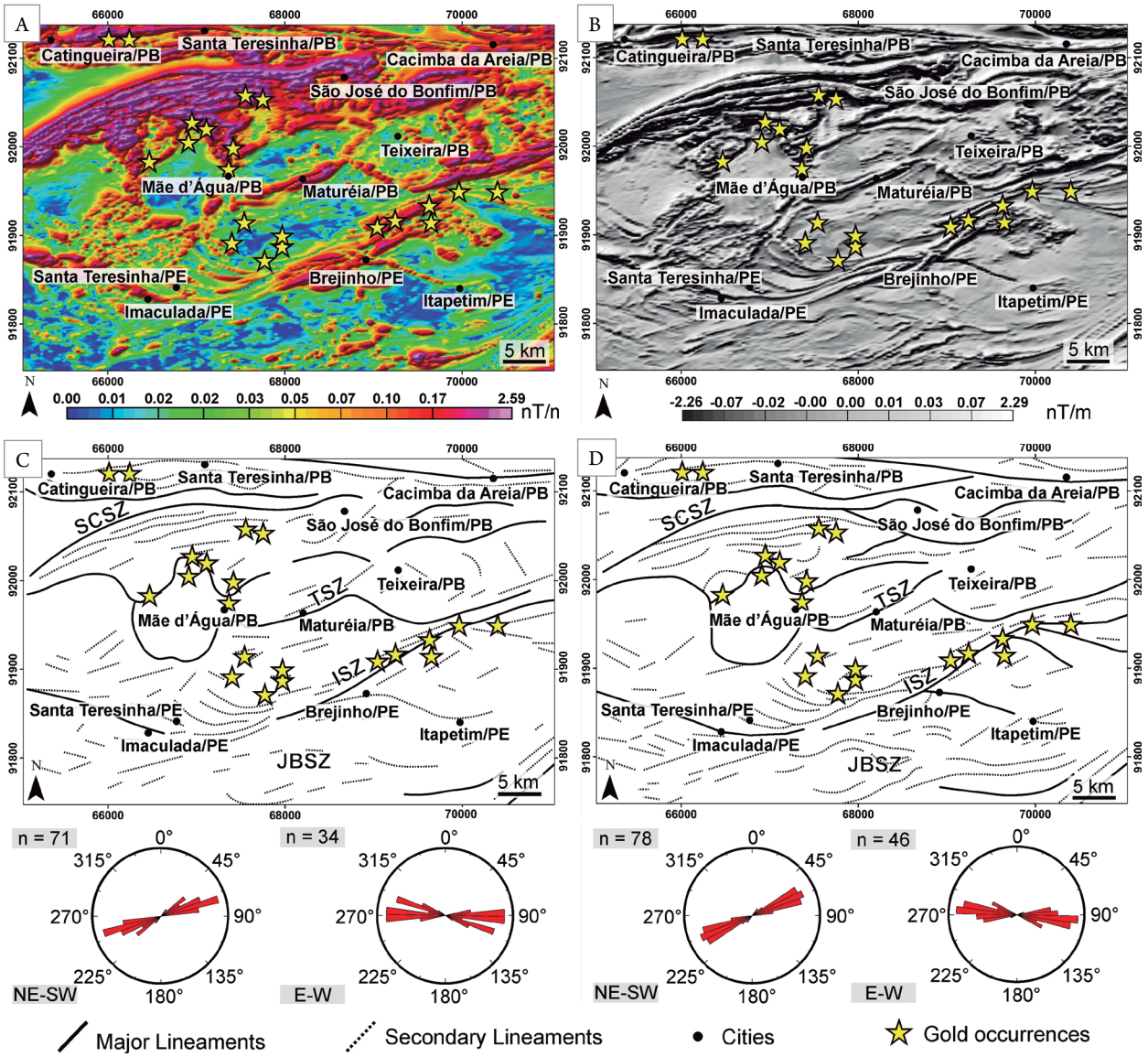

SCSZ: Serra do Caboclo Shear Zone; TSZ: Tendó Shear Zone; ISZ: Itapetim Shear Zone; JBSZ: Juru-Belém Shear Zone; PB: State of Paraíba; PE: State of Pernambuco.

Figure 3. Magnetic images of (A) analytic signal amplitude (ASA) and (B) first vertical derivative (DZ), and interpretation of magnetic lineaments from (C) ASA and (D) DZ images. Rose diagrams show NE-SW and E-W trends.

correlated with colluvium deposits shown in the geological map (Fig. 1B).

In the thorium map, the highest values (~ 14.00–60.67 ppm) are concentrated in the southern portion of the studied area and are mostly associated with the gneisses of Cariris Velhos Granitic Suite (Fig. 4B, domains 1 and 2). A significant part of gold occurrences associated with the ISZ is seen along a narrow and elongated body enriched in Th (~ 25–60 ppm; Fig. 4B, domain 2) and U (~ 4–9 ppm; Fig. 4C, domain 1). The weaker signatures in thorium measurements (< 0.17 ppm) are mostly associated with Teixeira Batholith, which present an inverse correlation with the potassium map.

In spite of the presence of the common streaking pattern caused by variations in atmospheric radon concentrations during data acquisition (Minty *et al.* 1997), the uranium map is characterized by high values along ISZ and Brejinho Pluton (~ 2.00–9.27 ppm), in which some gold occurrences were registered (Fig. 4C, domains 1 and 2).

K/eTh ratio map

Considering that the K/eTh ratio may reveal possible zones of hydrothermal alteration and mineralization (*e.g.*, Galbraith & Saunders 1983), the form of gold occurrence in Itapetim gold district was analyzed in K/eTh image, and two main patterns were distinguished. Pattern 1 is related to the gold occurrences in close association with Teixeira Batholith and characterized by zones showing extremely high values of K/eTh ratios (> 1,000, near to Mãe d'Água sector, Fig. 4D, domain 1). Pattern 2, however, is related to the gold mineralization occurring along ISZ and is linked to a narrow zone of intermediate to high values of K/eTh ratios (~ 500, Fig. 4D, domains 5 and 6). Both patterns repeat in other points of the studied area. For instance, Pattern 1 reappears along regions at the north and south borders of Teixeira Batholith, whose locations are indicated by domains 2, 3 and 4 in Figure 4D. Pattern 2, moreover, repeats in an area located to the south of ISZ, assigned as domain 7 in Figure 4D.

Ternary image and interpreted litho-geophysical map

For this study, the ternary image was used mainly for geological mapping purposes. Eleven litho-geophysical domains were classified according to the intensities (low, medium to low, medium, medium to high and high, see Tab. 1) on the three radioelements.

Despite some divergences, a comparison between the ternary image (Fig. 5A) with the geological map (Fig. 1B) permits

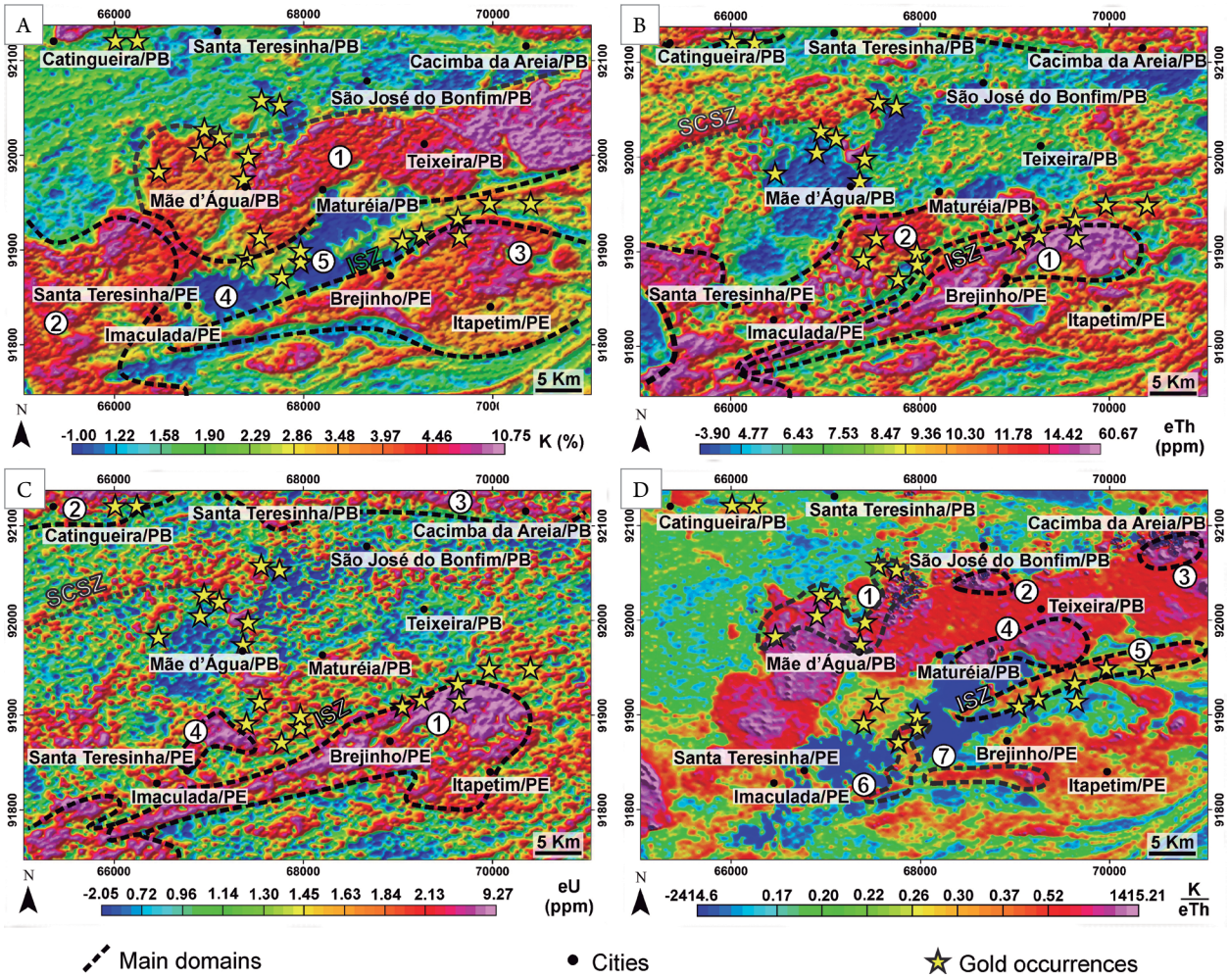

PB: State of Paraíba; PE: State of Pernambuco; ISZ: Itapetim Shear Zone; SCSZ: Serra do Caboclo Shear Zone.

Figure 4. Radiometric images of Itapetim gold district showing the location of gold occurrences and the main domains (1 to 7). (A) Potassium map. (B) Thorium map. (C) Uranium map. (D) K/eTh ratio. Numbers indicate domains relative to radiometric responses individually interpreted in each image.

to observe a spatial correlation regarding the litho-geophysical domains (Fig. 5B, Tab. 2) and lithological units. However, the ternary image also reveals its significance for this study for allowing to visualize internal variations within the units, not shown in previous geological mappings, their associations with important structures, and the combined behavior of the three radioelements in different gold mineralization sectors.

For instance, Teixeira Batholith is characterized by strong values of K, with some increment of medium to low counts of eTh and eU in its eastern segment (Fig. 5B, domains 1, 2 and 3).

Table 1. Intensities of radioelements used to define the qualitative interpretation of radiometric maps.

Intensities	K (%)	eTh (ppm)	eU (ppm)	K/eTh
Low	< 1.60	< 6.50	< 1.00	< 0.15
Medium	1.60–3.50	6.50–14.00	1.00–1.80	0.15–0.30
High	3.50–5.00	10.00–14.00	1.80–3.00	0.30–0.70
Very high	5.00–10.75	14.00–60.67	3.00–9.27	> 0.70

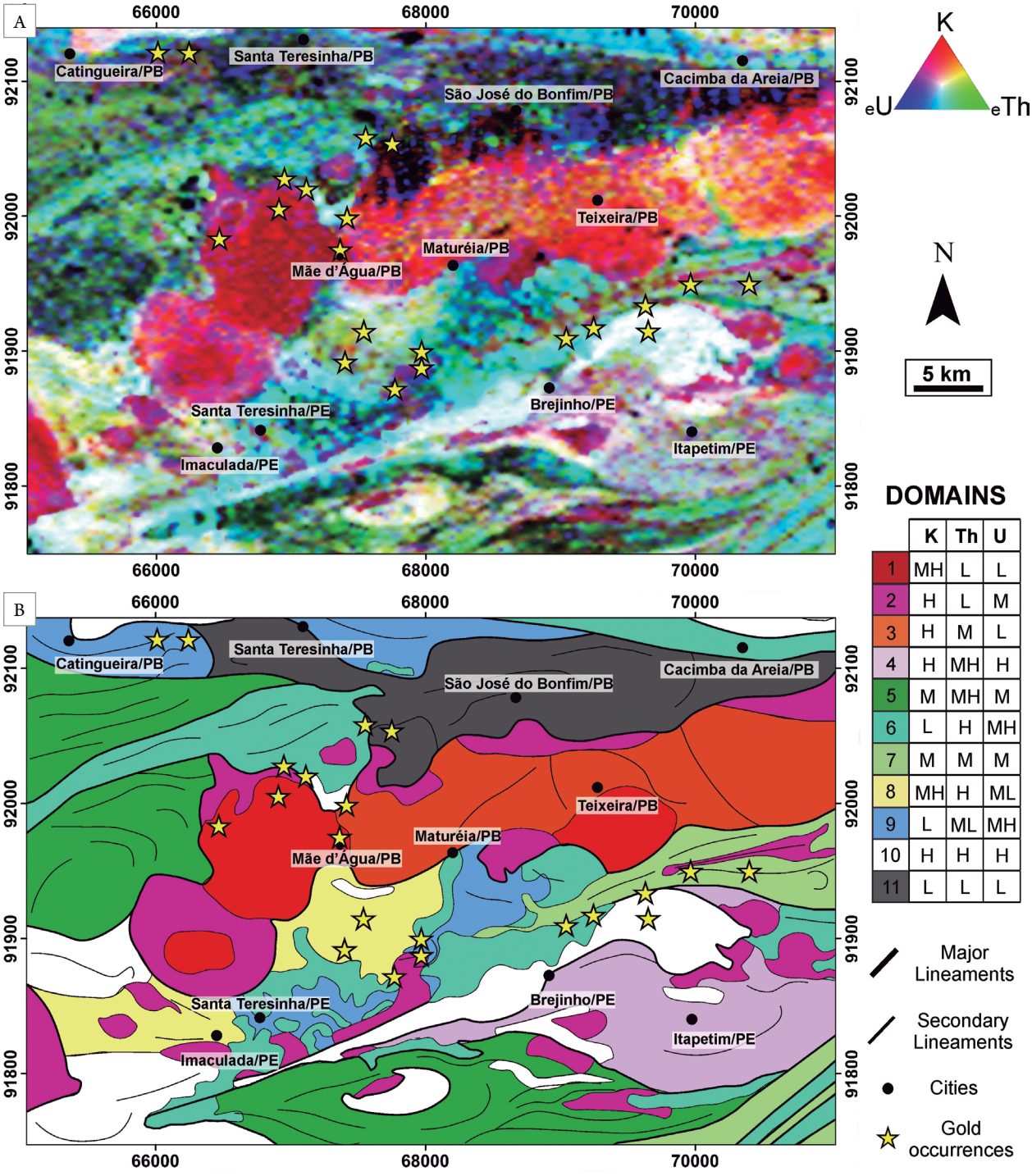

L: low; ML: medium to low; M: medium; MH: medium to high; H: high; PB: State of Paraíba; PE: State of Pernambuco.

Figure 5. (A) Ternary image (RGB composition) of K, eTh, and eU. (B) Litho-geophysical domains and radiometric lineaments.

The high counts on K are corroborated by the extensive presence of potassium feldspar (more than 30% in modal composition) and its shoshonitic affinity (Sial & Ferreira 2016). On the other hand, Brejinho Pluton shows intermediate to high counts of the three elements (Fig. 5B, domain 4). It has a monzogranitic composition and accessory minerals include epidote, apatite, titanite, and zircon. As seen in the ternary map, it is characterized by an elongated shape controlled by the ISZ.

The radiometric signature presented by the gneisses, which have monzogranitic to sienogranitic compositions from Cariris Velhos Granitic Suite (Santos 1995, Maia 2002), shows medium to high values of eTh associated with variations in eU (generally more expressive) and K contents (Fig. 5B, domains 6, 7, 8 and 9), appearing mostly in cyan, green or blue colors. The colluvial material deposited along those gneisses shows a substantial content of eTh and eU that indicate these rocks as probable sources, which is reflected in the composite map. Along the ISZ, these gneissic rocks show a significant increase in eU and K, appearing as whitish shades in the ternary image (Fig. 5B, domain 10).

The metasedimentary rocks also present variations in radiometric signatures. In certain regions (extreme south and northwest), they reveal a thorium-rich response (Fig. 5B, domains 5 and 6). Lastly, in the northern portion of the area, low counts of the three radioelements predominate (Fig. 5B, domain 11).

Structural analysis and mineral alteration description of Itapetim district

The general distribution of gold occurrences in the studied area is concentrated in the NE-SW and E-W directions along well-marked lineaments in the geophysical maps (Figs. 2 to 5). The E-W Patos Lineament is the most expressive structure of the region and forms a huge mylonitic corridor of several km wide. This structure is associated with the emplacement of major granitic rocks, including Teixeira Batholith, as well as the development of local migmatization and minor structural corridors. Nevertheless, additional geophysical lineaments show a strong correlation with NE-SW trending shear zones, *i.e.*, Itapetim, Serra do Caboclo, Tendó and Juru-Belém (see Fig. 1B). Mesoscopic and microscopic deformation markers are almost identical in all the NE-oriented shear zones, suggesting that they are coeval and developed in the same strain and crustal conditions. Thus, NE-SW oriented shear zones are ascribed as "Itapetim Shear System".

In the northern portion of the studied area, the dextral Patos Lineament together with the sinistral Serra do Caboclo Shear Zone make up a local conjugated strike-slip system, whose influence is observed along the metasedimentary rocks of Riacho Gravatá Complex and Santana dos Garrotes Formation. This is also associated with punctual gold occurrences in the northern portion of the studied area. Associated rocks show medium angled to sub-vertical ENE-WSW foliation planes that present low-plunging mineral stretching lineations. Variable kinematic criteria within this shear system include the presence of anastomosed millimetric foliation banding, S-C fabrics defined by phyllosilicate crystals alignments (Fig. 6A), rotated quartz porphyroclasts (Fig. 6B), and folded quartz ribbons.

The best-preserved gold-bearing rocks of the area are linked to Itapetim Shear System. In the region, it marks a narrow belt along rocks of Riacho do Forno, Recanto and São Caetano complexes, forming a 4 km wide and 40 km long mylonitic corridor between Teixeira and Brejinho granitic bodies. Mylonitic rocks associated with these shear systems are mostly characterized by planar- to plane-linear fabrics (S- to SL mylonites), displaying a well-preserved flat to anastomosed protomylonitic to mylonitic foliation planes (Fig. 7A). Such planes are locally folded and associated with parallel horizontal to sub-horizontal mineral stretching lineations that are marked by quartz-biotite-chlorite-epidote

Table 2. Detailed description of radiometric litho-geophysical domains interpreted in the study area.

Domains	Description
1	Potassium-rich domain located in Mãe d'Água sector and in the central portion of the western, following granitic body (to the north of Imaculada city).
2	Potassium-rich domain (with medium counts of eU) in the borders of Teixeira Batholith, in some small bodies widespread along Cariris Velhos Granitic Suite, and close to Brejinho Pluton.
3	Potassium-rich domain (with medium counts of eTh) widespread in the NE and central portion of Teixeira Batholith.
4	Potassium and uranium-rich domain defining great part of Brejinho Pluton.
5	Thorium-rich domain (with intermediate amounts of K and eU) in the south and NW portion of the area, respectively, associated with (1) São Caetano Complex and (2) Riacho Gravatá Complex and Santana dos Garrotes Formation.
6	Domain enriched in eTh and eU covering part of Riacho Gravatá Complex, areas of the Cariris Velhos Granitic Suite and colluvium material.
7	Domain showing intermediate values of radioelements (K, eTh and eU), located in the central NE portion of the area, covering part of Cariris Velhos Granitic Suite (Recanto Complex).
8	Thorium-rich domain (with intermediate amounts of K) along the coverage area of Cariris Velhos Granitic Suite (Riacho do Forno Complex).
9	Uranium-rich domain interpreted in the north portion of study area, associated with part of metasedimentary rocks from Santana dos Garrotes Formation and Riacho Gravatá Complex (at north), and to colluvium material (at south).
10	Domain enriched in K, eTh and eU, interpreted along ISZ, in two areas in SW region and in widespread small bodies close to Brejinho Pluton.
11	Domain showing a deficiency in radioelements (K, eTh and eU) present further north of study area, in part of metasedimentary rocks from Santana dos Garrotes Formation and Riacho Gravatá Complex.

alignments abundant in protomylonitic members (Fig. 7B), whilst oblique alignments is present but not numerous on orthoderived mylonites and, therefore, indicate lineation rotation during the shear development (Fig. 7C). Open to tight overturned symmetrical to asymmetrical folds are typical in zones of quartz-feldspar segregations. These structures present vertical to gentle plunging axial planes, in a lesser extent, sub-parallel to the mylonitic foliation and interpreted as syn-kinematic. Punctual chevron (Fig. 7D), ptygmatic and sheath folds occur in strongly deformed members of São Caetano Complex, which are suggestive of local crustal anatexis.

Reliable mesoscopic kinematic criteria are scarce and include S-C surfaces and σ-type feldspar porphyroclasts that are only observed in well-developed protomylonites. In contrast, well-preserved microtectonic markers are widespread. The most representative microstructures are S-C-C' surfaces, quartz ribbons, mica fish (predominately muscovite bents, Fig. 7E), and local kink bands. Recrystallization along shear planes, core-and-mantle structures and development of pressure shadows (Fig. 7F) are also present in zones where feldspar and quartz crystals are abundant. Quartz segregations are mostly characterized by neo-formed tiny grains that present well-developed undulose extinction, which is also present, but not common, in folded muscovite lamellae.

Dilatation structures including quartz-bearing, aplitic and pegmatitic veins are always present and closely related to mylonitic rocks. Although mineralization might occur along mylonitic foliation planes or hinge-lines of micro-folds, it is mostly associated with nucleated quartz or aplitic veins, especially with the presence of pyrite and arsenopyrite alignments (Figs. 8A and 8B), which might develop *boudins* and minor veinlets parallel or sub-parallel to mylonitic foliation planes (Fig. 8C). Discordant mineralized veinlets are also present.

Along the Itapetim and adjacent shear zones, quartz veins are mostly characterized by saccharoidal to massive textures (Fig. 8D). In general, these veins are associated with two different gangue mineral assemblages that are interpreted as the product of hydrothermal alteration and syn-tectonic deformation: quartz + potassium feldspar + tourmaline (Fig. 8E) and biotite + clinozoisite + epidote.

In the first paragenesis (most common), pink potassium feldspar is generally seen in association with quartz and tourmaline, which might show pegmatitic texture or disposition in micro-layers concordant to the mylonitic foliation (Fig. 8F). In thin section of veins, potassium feldspar is usually micro-fractured and altered to sericite or muscovite and shows dominantly, together with quartz, a polygonal arrangement (Fig. 9A). Tourmaline crystals are abundant and partially plastically deformed. Under microscope, they often exhibit a blue to green pleochroism (Fig. 9B), zoning in basal sections, and *augen* texture (Fig. 9C). They occur as coarse-grained crystal aggregates or micro-lenses (~ 0.1–1.0 mm thick), filling randomically oriented fractures along quartz veins. Moreover, in some occurrences, tourmaline is closely associated with tiny biotite crystals (~ 0.1 mm), as seen in Figure 9D.

The assemblage of biotite + clinozoisite + epidote, identified particularly in Santo Aleixo sector, might occur widespread in quartz veins matrix or filling fractures (Fig. 9E). Clinozoisite and epidote are observed mostly as anhedral grains (~ 0.2–1.0 mm), frequently showing zoning and micro-fractures. Subhedral biotite crystals, whose pleochroism varies from pale-yellow to green and, in other samples, from pale-yellow to reddish-brown, are related to them. Locally, well-developed crystals of chlorite, product of biotite alteration, are observed (Fig. 9F). Titanite is a common accessory mineral associated with the second mineral paragenesis, appearing usually close to biotite or chlorite crystals.

DISCUSSION

Lode-type gold deposits usually have close association with highly deformed regions, which might include one or more generations of faults or ductile shear zones (Groves *et al.* 2003, Suh *et al.* 2006, Holden *et al.* 2012, Wemegah *et al.* 2015). These structures are generally of continental scale and often act as conduits for hydrothermal fluids that transport a variety of metals, such as Au, Ag, As, Sb, Te, W, Mo, Bi, and B (McCuaig & Kerrich 1998, Groves *et al.* 2003, Condie & Pease 2008).

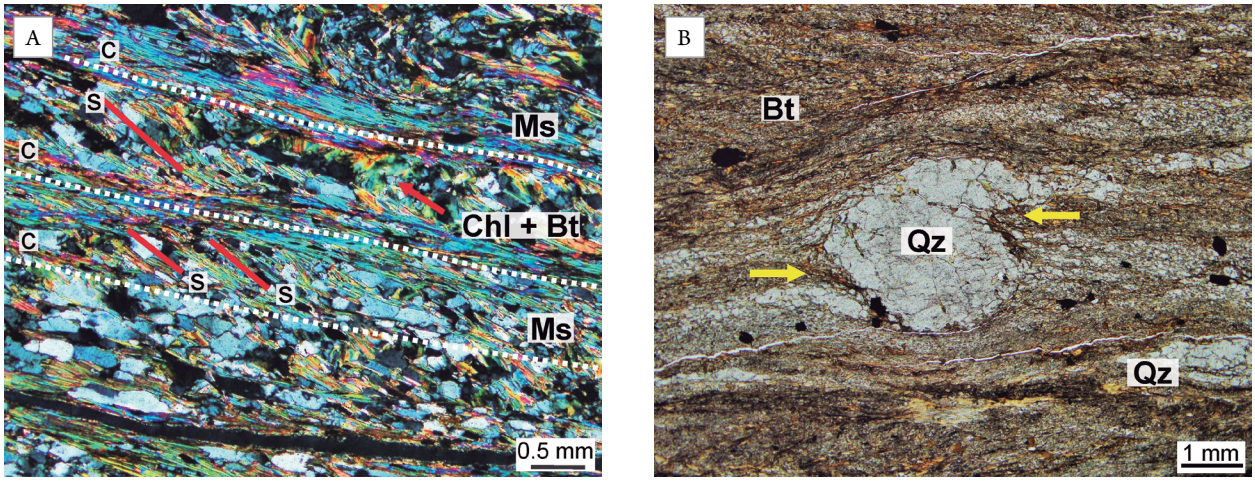

Bt: biotite; Chl: chlorite; Ms: muscovite; Qz: quartz.

Figure 6. Microscopic textures associated with mylonites of Serra do Caboclo Shear Zone: (A) Phyllite fabrics from Riacho Gravatá Complex, composed by muscovite, biotite, and chlorite presenting S-C fabrics (indicated by red lines and white dotted lines). (B) Type δ porphyroclast in quartz crystal from phyllonite of Riacho Gravatá Complex, showing sinistral strike-slip movement.

According to the magnetic image analysis, the main regional pathfinders related to the previously mapped gold sectors are strongly magnetized liner/curvilinear structures, including the major trace of Itapetim Shear System and the horsetail splays structures in its SW termination and the contact zone of Teixeira Batholith, specifically in Mãe d'Água sector (Figs. 3A and 3B). Magnetic susceptibly studies performed by Lima *et al.* (2000) and Archanjo *et al.* (2008) attributed the magnetic behavior observed along the contour of Teixeira Batholith as a result of magnetite formation during hydrothermal processes at shallow depths, which is in accordance with the paragenesis associated with the described gold-bearing rocks.

Those strongly magnetized areas represent reliable indicators of geological structures and, in field, are often linked to areas that underwent ductile and brittle deformation. Protomylonites and mylonites showing sub- to vertical dipping foliation

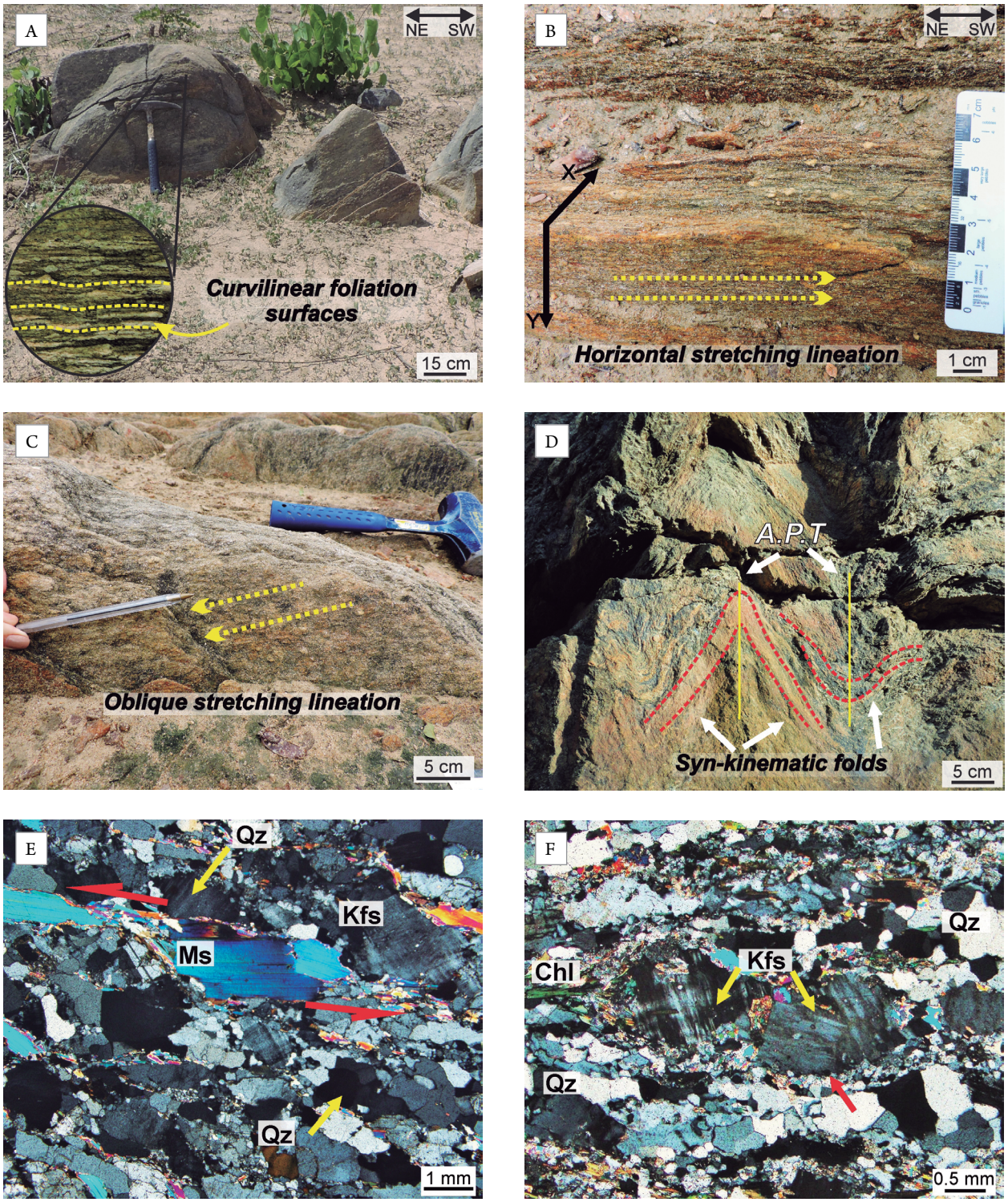

Chl: chlorite; Kfs: potassium feldspar; Ms: muscovite; Qz: quartz; A.P.T.: axial plane trace.

Figure 7. Structural characteristics of mylonitic rocks along Itapetim Shear Zone. (A) Overview of mylonite outcrop oriented in NE direction (70 Az/ 90º), and strike-slip foliation is marked by highly stretched crystals of quartz and feldspar. (B) Protomylonitic schist showing horizontal lineation. (C) Oblique oriented mineral stretching lineation in vertical foliation planes. (D) Syn-kinematic chevron folds with vertical- to subvertical axial planes. (E) Mica-fish marked by deformed muscovite crystal showing a piece of evidence of sinistral deformation. (F) Protomylonite showing augens of potassium feldspar (developing pressure shadow — red arrow) and quartz ribbons with polygonal texture.

characterize the most frequent types of rock, which present a set of structures indicative of deep-seated ductile deformation, such as micro-folds, quartz ribbons, type δ porphyroclasts, S-C fabrics, bent-flake mica fish, and shadow pressure texture. The brittle deformation phase is evidenced by fractures and micro-fractures (usually filled up with hydrothermal minerals as quartz and tourmaline), which reveal their importance since the formation of mineralized veins of the studied shear zones is associated with repeated episodes of hydrofracturing and circulation of hydrothermal fluids (crack-seal mechanism; Ramsay 1980, Maia 2002, Almeida 2003).

Indeed, magnetic data highly support that major shear zones control gold occurrences in the region. Foliation and lineation characteristics are suggestive of transcurrent corridors for gold percolation. Nevertheless, the presence of mylonites with oblique lineation and syn-kinematic NE-trending upright folds, even in the presence of vertical S-L mylonites, is interpreted in Borborema Province as strain partition of an initially protracted contractional regime (Neves *et al.* 2005). Thus, it is possible that the combination of contraction and strike-slip movements resulted in a transpressional regime that generated the studied shear zones.

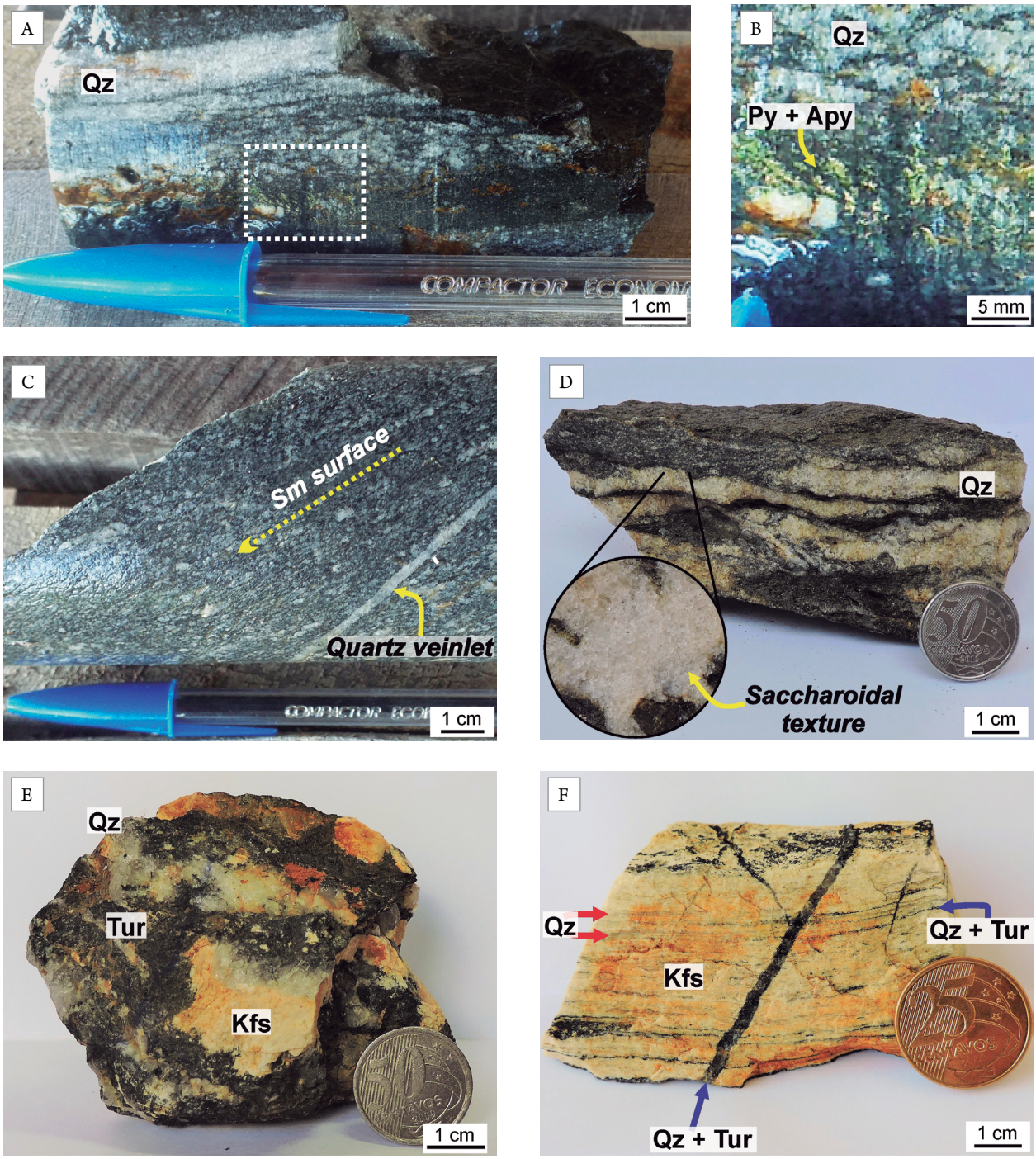

Apy: arsenopyrite; Kfs: potassium feldspar; Py: pyrite; Qz: quartz; Tur: tourmaline; Sm: mylonitic foliation.

Figure 8. Samples collected in mineralized areas. (A) Sample showing contact between quartz vein and mylonitic host rock, and layer composed by pyrite and arsenopyrite. (B) Zoom of sample shown in Figure 8A presenting fine layer of pyrite and arsenopyrite. (C) Host rock exhibiting mylonitic foliation marked by alignment of quartz crystals and presence of veinlet of quartz, parallel to the mylonitic foliation. (D) Quartz veins concordant to the mylonitic foliation exhibiting saccharoidal texture. (E) Aggregate of quartz, tourmaline, and potassium feldspar with pegmatitic texture. (E) Assemblage of quartz+tourmaline+potassium feldspar showing mylonitic texture.

According to all that has been described, based on the combination of magnetic data analysis as well as the recognition and geometric description of the region structures, strike-slip to transpressional shear zones and brittle faults that crosscut Teixeira Batholith are interpreted as the main pathways for the mineralized fluids, as early suggested by Lima *et al.* (2000).

Regarding the usage of airborne gamma-ray applied to gold prospecting, the contrasting behavior or antagonism between the K and Th radioelements defined by Ostrovskiy (1975) has been represented as a chief parameter. In fact, since its conception, this relationship became one of, if not the main, pathfinders in gold prospective studies involving this methodology, and the K/eTh (or eTh/K) map has been exhaustively used (*e.g.*, Shives *et al.* 2000, Quadros *et al.* 2003, Almasi *et al.* 2015, Ohioma *et al.* 2017). The key feature recognized are, in general, zones of hydrothermal alteration evidenced by an increase of K even in high-potassium host rocks (Hoover & Pearce 1990).

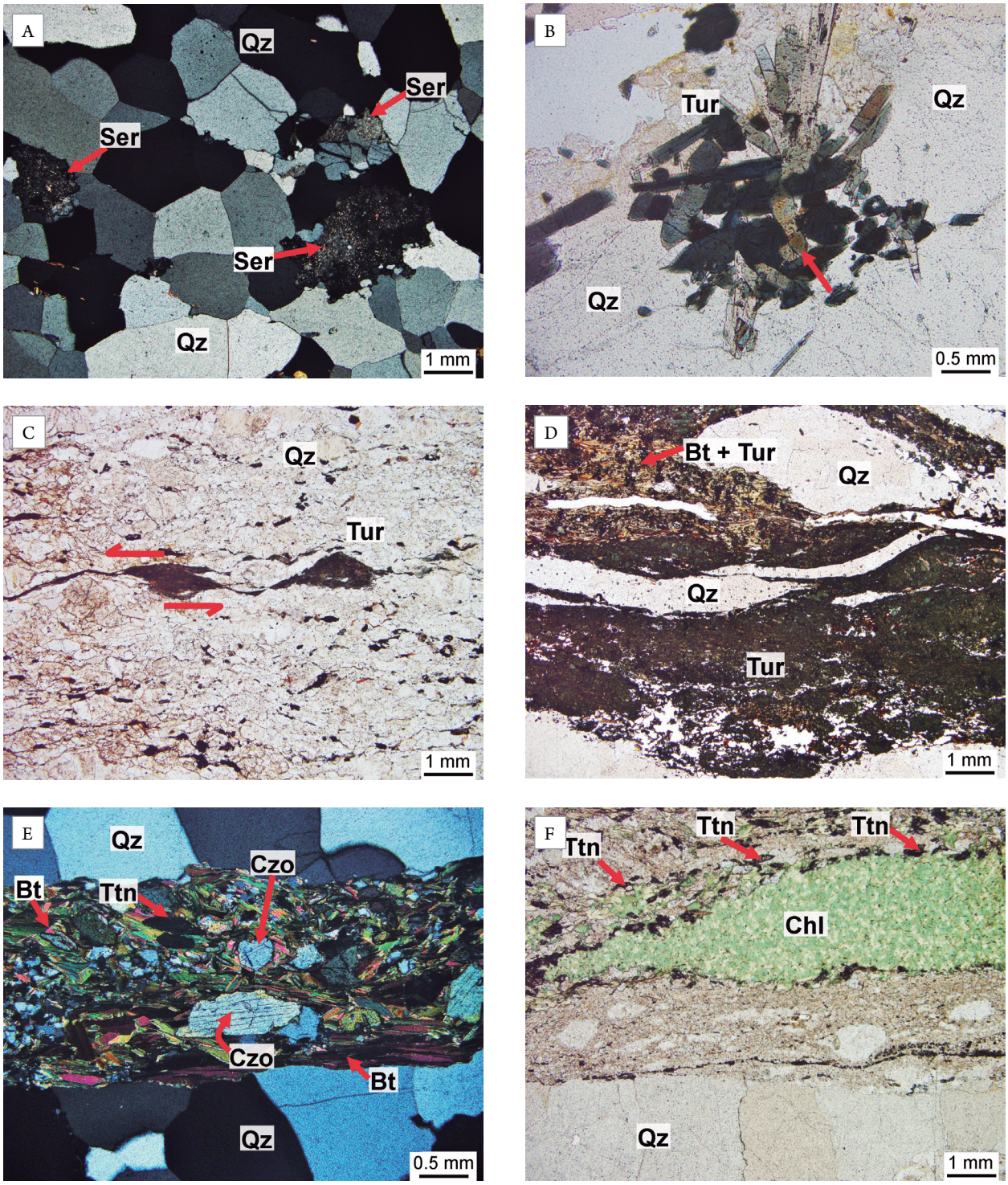

Bt: biotite; Chl: chlorite; Czo: clinozoisite; Ms: muscovite; Qz: quartz; Ser: sericite; Ttn: titanite; Tur: tourmaline.

Figure 9. Microscopic aspects of hydrothermal minerals in Itapetim gold district. (A) Sample of quartz vein showing a polygonal arrangement, containing crystals of potassium feldspar almost completely transformed into sericite (see red arrows). (B) Aggregate of prismatic tourmaline crystals, in quartz vein, exhibiting a blue to green pleochroism. Zoning is observed in basal section (see red arrow). (C) Quartz vein containing tourmaline porphyroclasts (type σ) evidencing sinistral deformation. (D) Quartz vein showing the association of biotite (in tiny crystals) and tourmaline. (E) Assemblage of Bt + Czo + Ep, observed in Santo Aleixo Sector, filling fracture in quartz vein. (F) Layer composed by chlorite, product of biotite alteration, in quartz vein. Small crystals of titanite are seen right in contact with chlorite (see red arrows).

In Itapetim gold district, Coutinho (1994) pointed out a substantial enrichment of K in mineralized areas (resultant of hydrothermal alteration) unveiled by a mineral assemblage dominated by tourmaline and potassium feldspar (similarly found in this study; Figs. 8D and 8E). Other evidence, observed herein, that attest the occurrence of hydrothermal alteration are the biotite chloritization, the blue-green pleochroism shown by tourmaline (typical of the hydrothermal varieties, Charoy 1979), and the transformation of potassium feldspar into sericite or muscovite. Particularly for the replacement of feldspar by sericite or muscovite, mass balance studies (*e.g.*, Craw *et al.* 2009, Li *et al.* 2013, Abdelnasser *et al.* 2014) have reported the possibility of a K_2O gain during those transformations, which might have also contributed to an increase in the amount of this radioelement in the studied area.

In the potassium and K/eTh ratio images, this K enrichment along ISZ and Teixeira Batholith (Figs. 4A and 4B) was seen. Considering the pattern of gold occurrence found in the K/eTh ratio image (high values of K/eTh ratios > 500), the zones where they recur were interpreted as potential hydrothermally altered areas, enabling gold mineralization.

The ternary image of K, eTh and eU (Fig. 5A) permits visualizing, in a general panel, the behavior of the three radioelements in the studied area, allowing the individualization of some geological units, despite the existence of internal variation in some of them. From the perspective of this image, the gold occurrences are largely related to domain 2 (Fig. 5B), whose K content varies between medium and high values (~ 3.5–7.0 %).

Therefore, the most precise pathfinder for the gold occurrences, in the studied area, is their association with structured zones. However, there is also a good correlation between the K content and the mineralized areas (remarkably in K and K/eTh maps). Thus, regarding these aspects, we produced an integrated map (fusion of DZ and ternary images) depicting the main results of airborne magnetic and gamma-ray spectrometric interpretation (lineaments and few radiometric domains of ternary and K/eTh ratio images) to locate new gold target areas. In this map, ten new zones of possible gold mineralization are indicated, based on the combined analysis of geophysical and geological features presented herein (Fig. 10).

Within the Borborema Province, similar gold deposits are Neoproterozoic and occur in Seridó Belt (Northern Borborema Province, Araújo *et al.* 2002). $^{40}Ar/^{39}Ar$ geochronological data from mica grains point out that the minerals associated with gold occurrences are mostly Cambro-Ordovincian (520–506 Ma), which is a fair estimation of shear zone development. It indicates that late gold concentration in Borborema Province occurred in the last stages of Brasiliano-Pan African orogeny (Araújo *et al.* 2005). In West Africa, correlative lode-type gold occurrences are also reported, including those from

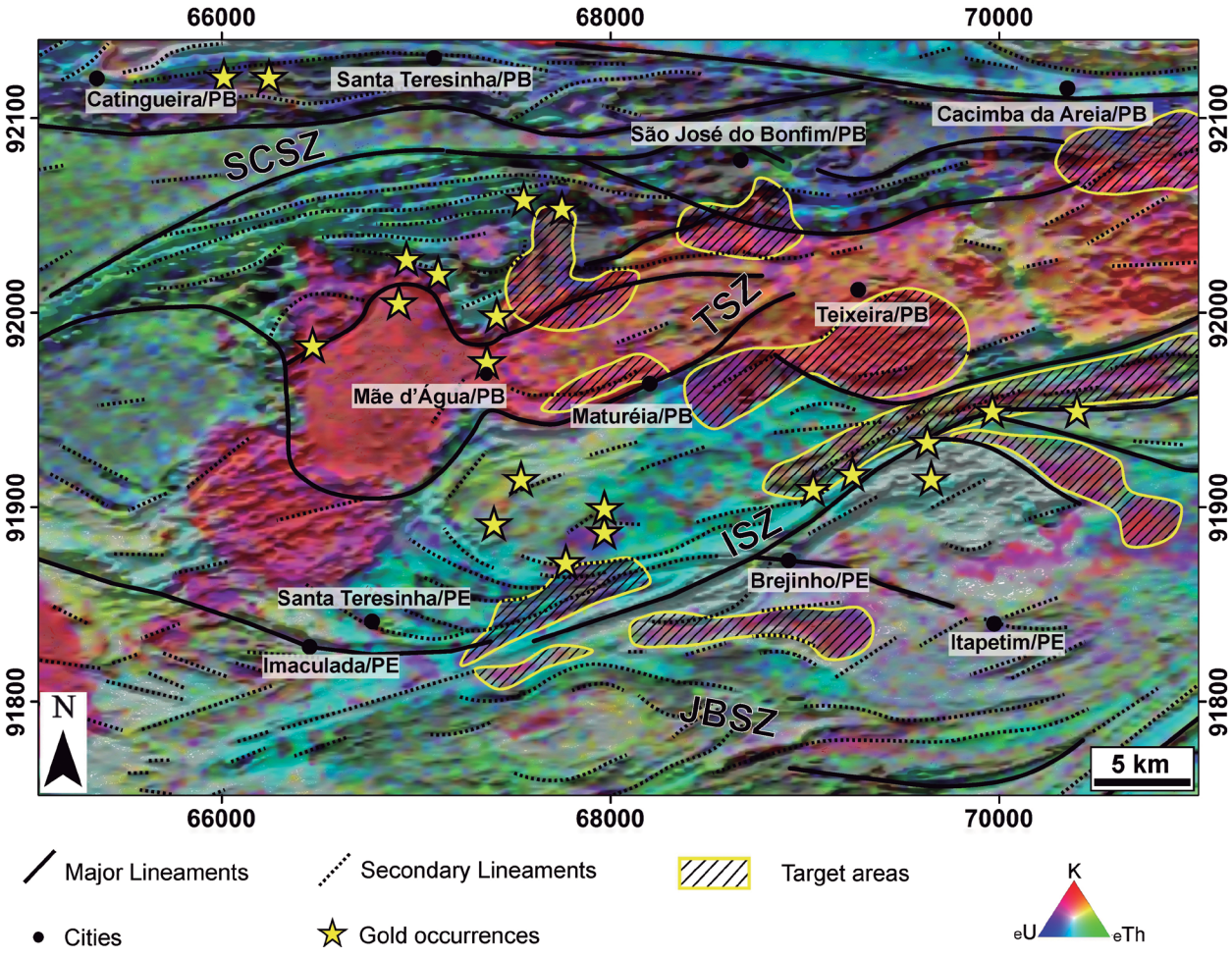

SCSZ: Serra do Caboclo Shear Zone; TSZ: Tendó Shear Zone; ISZ: Itapetim Shear Zone; JBSZ: Juru-Belém Shear Zone.

Figure 10. Integrated map (fusion of DZ and ternary images) showing the main interpretations made from airborne magnetic and gamma-ray spectrometric data. The hatched zones represent favorable areas for gold mineralization, considering the main pathfinders identified in the study area.

Central African Belt, such as Dimako-Mboscorro Deposit. Associated rocks occur within wide developed shear zone corridors (Njome & Suh 2005) that probably extends from central Africa, across the Atlantic, into NE Brazil related gold-bearing rocks, such as those from Itapetim (Suh *et al.* 2006, Takodjou Wambo *et al.* 2018).

CONCLUSIONS

This contribution presents an integrated analysis of airborne magnetic and gamma-ray spectrometric data of Itapetim gold district allied to the main field aspects observed in the mineralized areas.

The magnetic data revealed the occurrence of major and secondary lineaments disposed mainly in NE-SW and E-W, which correlates spatially to the most significant structures of the studied area: Patos Lineament, Serra do Caboclo and Itapetim shear zones. They also indicated that gold occurrences are associated with strongly magnetized areas, whose locations in the field correspond to ductile and brittle deformed regions containing protomylonitic and mylonitic rocks, eventually affected by fractures, in which hydrothermal fluids passed through and were crystalized as mineralized veins.

The major mesoscopic structural aspects of the gold-bearing protomylonites and mylonites include sub- to vertical dipping foliation, local folding and horizontal to sub-horizontal mineral stretching lineation. Microscopic features comprise, among others, quartz ribbons, mica fish, kink bands and core-and-mantle structures, besides the common fracturing observed in minerals (*e.g.*, potassium feldspar, tourmaline and clinozoisite) found in quartz veins.

Regarding the gamma-ray spectrometric data, we visualized the magnitude of each radiometric element and their behavior in ternary image, which permitted to identify the main sites of K enrichment. Part of those areas shows an abundant presence of potassium-rich hydrothermal minerals, such as tourmaline, potassium feldspar and sericite, occurring mainly in filling up fractures in quartz veins.

The airborne geophysical data (ternary composition and DZ images) were integrated in single map, and ten target areas were selected based on the presence of structures (interpreted by the presence of magnetic and radiometric lineaments) and possible hydrothermal alteration zones (inferred by potassium enrichment). This type of methodology showed its importance by providing unexpansive information of a broad mineralized area and supplying the geological dataset of Itapetim region for future gold prospective campaigns.

ACKNOWLEDGEMENTS

The authors are grateful to Coordenação de Aperfeiçoamento de Pessoal de Nível Superior (CAPES) for the scholarship and Programa de Pós-graduação em Geociências (PPGEOC) of Departamento de Geologia from Universidade Federal de Pernambuco (UFPE) for their financial support. We also thank the Laboratório de Gemologia (LABGEM — UFPE) and its collaborators, for the use of microscopes, and the Serviço Geológico do Brasil (CPRM) for providing the geophysical data used in this study.

ARTICLE INFORMATION

Manuscript ID: 20190028. Received on: 04/16/2019. Approved on: 06/19/2019.

L. P. structured the manuscript, interpreted the geophysical data, described the petrographic data, prepared the figures and wrote the first draft of the manuscript, which is part of her master's degree thesis. L. S. supported the field work, structural interpretation and manuscript writing. T. C. aided the geophysical interpretations, revised and improved the manuscript.

Competing interests: The authors declare no competing interests.

REFERENCES

Abdelnasser A., Kumral M., Zoheir B., Weihed P., Kiran Y.D., Karaman M. 2014. Hydrothermal alteration geochemistry of Atud gold deposits at the central block of the Egyptian Eastern Desert, Egypt: Insights provided by mass-balance calculations. *In:* Goldschmidt Conference, Sacramento, California. *Goldschmidt Abstracts…*, p. 8-13.

Airo M.L. 2002. Aeromagnetic and Aeroradiometric Response to Hydrothermal Alteration. *Surveys in Geophysics*, **23**(4):273-302. https://doi.org/10.1023/A:1015556614694

Airo M.L. & Mertanen S. 2008. Magnetic signatures related to orogenic gold mineralization, Central Lapland Greenstone Belt, Finland. *Journal of Applied Geophysics*, **64**(1-2):14-24. https://doi.org/10.1016/j.jappgeo.2007.10.003

Almasi A., Jafarirad A., Afzal P., Rahimi M. 2015. Prospecting of gold mineralization in Saqez area (NW Iran) using geochemical, geophysical and geological studies based on multifractal modelling and principal component analysis. *Arabian Journal of Geosciences*, **8**(8):5935-5947. https://doi.org/10.1007/s12517-014-1625-2

Almeida F.F., Hasui Y., Brito Neves B.B., Fuck R.A. 1981. Brazilian structural provinces: an introduction. *Earth Sciences Reviews*, **17**(1-2):1-29. https://doi.org/10.1016/0012-8252(81)90003-9

Almeida H.L. 2003. *Estudo microestrutural em mineralização aurífera do tipo-veio hospedada em zona de cisalhamento: caso do depósito Sertãozinho, Província Borborema, NE do Brasil*. PhD Thesis, Universidade Estadual Paulista "Júlio de Mesquita Filho", Rio Claro, São Paulo, 103 p.

Araújo M.N.C., Alves da Silva F.C., Jardim de Sá E.F., Holcombe R.J. 2002. Geometry and structural control of Au Vein mineralizations In the Seridó Belt, Northeastern Brazil. *Journal of South American Earth Sciences*, **15**(3):337-348. https://doi.org/10.1016/S0895-9811(02)00040-8

Araújo M.N.C., Vasconcelos P.M., Alves da Silva F.C., Jardim de Sá E., Sá J.M. 2005. $^{40}Ar/^{39}Ar$ geochronology of gold mineralization in Brasiliano strike-slip shear zone in the Borborema Province, NE Brazil. *Journal of South American Earth Sciences*, **19**(4):445-460. https://doi.org/10.1016/j.jsames.2005.06.009

Archanjo C.J., Hollanda M.H.B.M., Rodrigues S.W., Neves B.B.B., Armstrong R. 2008. Fabrics of pre- and syntectonic granite plutons and chronology of shear zones in the Eastern Borborema Province, NE Brazil. *Journal of Structural Geology*, **30**(3):310-336. https://doi.org/10.1016/j.jsg.2007.11.011

Basto C.F., Caxito F.A., Vale J.A.R., Silveira D.A., Rodrigues J.B., Alkmim A.R., Valeriano C.M., Santos E.J. 2019. An Ediacaran back-arc basin preserved in the Transversal Zone of the Borborema Province: Evidence from geochemistry, geochronology and isotope systematics of the Ipueirinha Group, NE Brazil. *Precambrian Res.*, **320**:213-231. https://doi.org/10.1016/j.precamres.2018.11.002

Baumgartner R., Romer R.L., Moritz R., Sallet R., Chiaradia M. 2006. Columbite-tantalite-bearing granitic pegmatites from the Seridó Belt, northeastern Brazil: Genetic constraints from U-Pb dating and Pb isotopes. *Canadian Mineralogist*, **44**(1):69-86. http://doi.org/10.2113/gscanmin.44.1.69

Bedini E., Rasmussen T.M. 2018. Use of airborne hyperspectral and gamma-ray spectroscopy data for mineral exploration at the Sarfartoq carbonatite complex, southern West Greenland. *Geosciences Journal*, **22**(4):641-651. https://doi.org/10.1007/s12303-017-0078-5

Bittar S.M.B. 1998. *Faixa Piancó-Alto Brígida: Terrenos tectono-estratigráficos sob regimes metamórficos e deformacionais contrastantes*. PhD Thesis, Institute of Geosciences, Universidade de São Paulo, São Paulo, 126 p.

Brazilian Geological Survey (CPRM). 1984. Projeto Itapetim, PE/PB Setor Sertãozinho Plano de Lavra Experimental: Alvarás 4282, 5296, 5353, 5413/83. Internal report. Rio de Janeiro, CPRM.

Brito Neves B.B., Fuck R.A., Pimentel M.M. 2014. The Brasiliano collage in South America: a review. *Brazilian Journal of Geology*, **44**(3):493-518. http://dx.doi.org/10.5327/Z2317-4889201400030010

Brito Neves B.B., Santos E.J., Fuck R.A., Santos L.C.M.L. 2016. A preserved early Ediacaran magmatic arc at the northernmost portion of the Transversal Zone central subprovince of the Borborema Province, Northeastern South American. *Brazilian Journal of Geology*, **46**(4):491-508. http://dx.doi.org/10.1590/2317-4889201620160004

Brito Neves B.B., Santos E.J., Schmus W.R.Q. 2000. Tectonic history of the Borborema province. In: Cordani U.G., Milani E.J., Thomaz-Filho A., Campos D.A. (eds.), Tectonic Evolution of South America. *31st International Geological Congress*, Rio de Janeiro. *Special Publication …*, p. 151-182.

Charoy B. 1979. *Definition et importance des phenomenes deutériques et des fluids associés dans les granites: conséquences métallogeniques*. PhD Thesis, Institut National Polytechnique de Lorraine, Nance, 366 p. Available at: <http://www.sudoc.fr/042232392>. Accessed on: March 14, 2019.

Craw D., Upton P., Mackenzie D. 2009. Hydrothermal alteration styles in ancient and modern orogenic gold deposits, New Zealand. *New Zealand Journal of Geology and Geophysics*, **52**(1):11-26. https://doi.org/10.1080/00288300909509874

Condie K.C. & Pease V. 2008. When did plate tectonics begin on planet Earth? *Geological Society of America*, **440**:281-294. https://doi.org/10.1130/SPE440

Cordani U.G., Pimentel M.M., Araújo C.E.G., Fuck R.A. 2013. The significance of the Transbrasiliano-Kandi tectonic corridor for the amalgamation of West Gondwana. *Brazilian Journal of Geology*, **43**(3):583-597. http://dx.doi.org/10.5327/Z2317-48892013000300012

Costa F.G., Palheta E.S.M., Rodrigues J.B., Gomes I.P. Vasconcelos A.M. 2015. Geochemistry and U–Pb zircon ages of plutonic rocks from the Algodões granite-greenstone terrane, Tróia Massif, northern Borborema Province, Brazil: Implications for Paleoproterozoic subduction-accretion processes. *Journal of South American Earth Sciences*, **59**:45-68. https://doi.org/10.1016/j.jsames.2015.01.007

Coutinho M.G.N. 1994. *The geology of shear-zone hosted gold deposits in Northeast Brazil*. PhD Thesis, London University, London, 391 p.

Coutinho M.G.N. & Alderton D.H.M. 1998. Character and genesis of Proterozoic shear zone-hosted gold deposits in Borborema Province, northeast Brazil. *Transactions Institution of Mining Metallurgy (Section B: Applied Earth Sciences)*, **107**:109-119.

Dantas E.L., Souza Z.S., Wernick E., Hackspacher P.C., Martin H., Xiadong D., Li J.W. 2013. Crustal growth in the 3.4-2.7 Ga São José do Campestre Massif, Borborema Province, NE Brazil. *Precambrian Research*, **227**:120-156. https://doi.org/10.1016/j.precamres.2012.08.006

Dickson B. & Scott K.M. 1997. Interpretation of aerial gamma-ray surveys - adding the geochemical factors. *AGSO Journal of Australian Geology & Geophysics*, **17**:187-199.

Ferreira C.A. & Santos E.J. 2000. *Programa Levantamentos Geológicos Básicos do Brasil:* Jaguaribe SE - Folha SC. 24-Z. Estados do Ceará, Rio Grande do Norte, Paraíba e Pernambuco. Escala 1:500.000. Geologia e metalogênese. Texto explicativo. Recife, CPRM, 121 p.

Galbraith J.H. & Saunders D.F. 1983. Rock classification by characteristics of aerial gamma ray measurements. *Journal of Geochemical Exploration*, **18**(1):49-73. https://doi.org/10.1016/0375-6742(83)90080-8

Ganade de Araújo C.E., Cordani U.G., Weinberg R.F., Basei M.A., Armstrong R., Sato K. 2014. Tracing Neoproterozoic subduction in the Borborema Province (NE-Brazil): Clues from U-Pb geochronology and Sr-Nd-Hf-O isotopes on granitoids and migmatites. *Lithos*, **202-203**:167-189. https://doi.org/10.1016/j.lithos.2014.05.015

Goldfarb R.J. & Groves D.I. 2015. Orogenic gold: common or evolving fluid and metal 702 sources through time. *Lithos*, **223**:2-26. https://doi.org/10.1016/j.lithos.2015.07.011

Groves D.I. & Santosh M. 2015. Province-scale commonalities of some world-class gold deposits: implications for mineral exploration. *Geoscience Frontiers*, **6**(3):389-399. https://doi.org/10.1016/j.gsf.2014.12.007

Groves D.I., Goldfarb R.J., Robert F., Hart C.J.R. 2003. Gold deposits in metamorphic belts: overview of current understanding, outstanding problems, future research, and exploration significance. *Economic Geology*, **98**(1):1-29. https://doi.org/10.2113/gsecongeo.98.1.1

Groves D.I., Santosh M., Goldfarb R.J., Zhang L. 2018. Structural geometry of orogenic gold deposits: Implications for exploration of world-class and giant deposits. *Geoscience Frontiers*, **9**(4):1163-1177. https://doi.org/10.1016/j.gsf.2018.01.006

Holden E.J., Wong J.C., Kovesi P., Wedge D., Dentith M., Bagas L. 2012. Identifying structural complexity in aeromagnetic data: An image analysis approach to greenfields gold exploration. *Ore Geology Reviews*, **46**:47-59. https://doi.org/10.1016/j.oregeorev.2011.11.002

Hollanda M.H.B.M., Souza Neto J.A., Archanjo C.J., Stein H., Maia A.C.S. 2017. Age of the granitic magmatism and the W-Mo mineralizations in skarns of the Seridó belt (NE, Brazil) based on zircon U-Pb (SHRIMP) and Re-Os determinations. *Journal of South American Earth Sciences*, **79**:1-11. https://doi.org/10.1016/j.jsames.2017.07.011

Hoover D.B. & Pierce A.A. 1990. Annotated bibliography of gamma-ray methods applied to gold exploration. *Open-File Report*. U.S. Geological Survey, 90-203, 23p. https://doi.org/10.3133/ofr90203

Hronsky J.M.A. & Groves D.I. 2008. Science of targeting: definition, strategies, targeting and performance measurement. *Australian Journal of Earth Sciences*, **55**(1):3-12. https://doi.org/10.1080/08120090701581356

LASA Engenharia e Prospecções S/A & PROSPECTORS Aerolevantamentos e Sistemas LTDA. 2009. *Projeto Aerogeofísico Paraíba - Rio Grande do Norte; Pernambuco - Paraíba:* relatório final do levantamento e processamento dos dados magnetométricos e gamaespectométricos. Internal report. Rio de Janeiro, Lasa Engenharia e Prospecções; Prospectors Aerolevantamentos e Sistemas. Programa Geologia do Brasil (PGB).

Li X. 2006. Understanding 3D analytic signal amplitude. *Geophysics*, **71**(2):L13-L16. https://doi.org/10.1190/1.2184367

Li X.-C., Fan H., Santosh M., Hu F-F., Yang K-F., Lan T.-G. 2013. Hydrothermal alteration associated with Mesozoic granite-hosted gold mineralization at the Sanshandao deposit, Jiaodong Gold Province, China. *Ore Geology Reviews*, **53**:403-421. https://doi.org/10.1016/j.oregeorev.2013.01.020

Lima H., Pimentel M., Santos L., Dantas, E. 2019. Isotopic and geochemical characterization of the metavolcano-sedimentary rocks of the Jirau do Ponciano dome: A structural window to a Paleoproterozoic continental ARC root within the Southern Borborema province, Northeast Brazil. *Journal of South American Earth Sciences*, **90**:54-69. https://doi.org/10.1016/j.jsames.2018.12.002

Lima R.G., Archanjo C.J., Macedo J.W.P., Melo Jr. G. 2000. Anomalias de suscetibilidade magnética no batólito granítico de Teixeira (Província da Borborema, Nordeste do Brasil) e sua relação com a zona de cisalhamento de Itapetim. *Revista Brasileira de Geociências*, **30**(4):685-692. http://dx.doi.org/10.25249/0375-7536.2000304685692

Lin-ping H. & Zhi-ning G. 1998. Discussion on "Magnetic interpretation using the 3-D analytic signal" (Walter R. Roest, Jacob Verhoef, and Mark Pilkington: Geophysics, 57, 116-125). *Geophysics*, **63**:667-670. https://doi.org/10.1190/1.1444366

Luiz-Silva W., Michel Legrand J., Xavier R. 2000. Composição e evolução dos fluidos no Depósito Aurífero São Francisco, Faixa Seridó, Província Borborema, Nordeste do Brasil. *Revista Brasileira de Geociências*, **30**(4):579-588. http://dx.doi.org/10.25249/0375-7536.2000304579588

Madrucci V., Veneziani P., Paradella W.R. 2003. Caracterização geológica e estrutural através da interpretação do produto integrado TM-Landsat 5 e dados aerogamaespectrométricos, região de Alta Floresta - MT. *Revista Brasileira de Geofísica*, **21**(3):219-234. http://dx.doi.org/10.1590/S0102-261X2003000300002

Maia H.N. 2002. *Deformação e fluxo de fluidos em zonas de cisalhamento: a integração de estudos estrutural, inclusões fluidos e isótopos estáveis dos veios mineralizados em ouro posicionados na zona de cisalhamento de Itapetim (NE do Brasil)*. PhD Thesis, Universidade Estadual de Campinas, Campinas, 204 p.

McCuaig T. & Kerrich R. 1998. P-T-t-deformation-fluid characteristics of lode gold deposits: Evidence from alteration systematics. *Ore Geology Reviews*, **12**(6):381-453. https://doi.org/10.1016/S0169-1368(98)80002-4

Medeiros V.C. 2004. *Evolução Geodinâmica dos Terrenos Piancó-Alto Brígida e Alto Pajeú, Domínio da zona Transversal, NE do Brasil*. PhD Thesis, Universidade Federal do Rio Grande do Norte, Natal, 198 p.

Metelka V., Baratoux L., Naba S., Jessell M.W. 2011. A geophysically constrained litho-structural analysis of the Eburnean greenstone belts and associated granitoid domains, Burkina Faso, West Africa. *Precambrian Research*, **190**(1-4):48-69. https://doi.org/10.1016/j.precamres.2011.08.002

Milligan P.R., Gunn P.J. 1997. Enhancement and presentation of airborne geophysical data. *AGSO Journal of Australian Geology and Geophysics*, **17**(2):63-75. Available at: <https://inis.iaea.org/search/search.aspx?orig_q=RN:28049084>. Accessed on: February 20, 2019.

Minty B.R.S., Luyendyk A.P.G., Brodie R.C. 1997. Calibration and data processing for airborne geophysical data. *ASGO Journal of Australian Geology & Geophysics*, **17**(2):51-62. Available at: <https://inis.iaea.org/search/search.aspx?orig_q=RN:28049083>. Accessed on: March 05, 2019.

Neves S.P. 2003. Proterozoic history of the Borborema Province (NE Brazil): correlations with neighboring cratons and Pan-African belts, and implications for the evolution of western Gondwana. *Tectonics*, **22**(4):1031-1044. https://doi.org/10.1029/2001TC001352

Neves S.P. 2018. Comment on "A preserved early Ediacaran magmatic arc at the northernmost part of the transversal zone - central domain of the Borborema Province, Northeast of South America", by B. B. de Brito Neves *et al.* (2016). *Brazilian Journal of Geology*, **48**(3):623-630. http://dx.doi.org/10.1590/2317-4889201820180049

Neves S.P., Bruguier O., Vauchez A., Bosch D., Silva J.M.R., Mariano G. 2006. Timing of crustal formation, deposition of supracrustal sequences and Transamazonian and Brasiliano metamorphism in easter Borborema Province (BE Brazil): Implications for western Gondwana assembly. *Precambrian Research*, **149**(3-4):197-216. https://doi.org/10.1016/j.precamres.2006.06.005

Neves S.P., Silva J.M.R., Mariano G. 2005. Oblique lineations in orthogneisses and supracrustal rocks: vertical partitioning of strain in a hot crust (Borborema Province, NE Brazil). *Journal of Structural Geology*, **27**(8):1513-1527. https://doi.org/10.1016/j.jsg.2005.02.002

Njome M.S. & Suh C.E. 2005. Tectonic evolution of the Tombel graben basement, southwestern Cameroon. *Episodes*, **28**(1):37-41.

Ohioma J.O., Ezomo F.O., Akinsunmade A. 2017. Delineation of Hydrothermally Altered Zones that Favour Gold Mineralization in Isanlu Area, Nigeria Using Aeroradiometric Data. *International Annals of Science*, **2**(1):20-27. https://doi.org/10.21467/ias.2.1.20-27

Oskooi B. & Abedi M. 2015. An airborne magnetometry study across Zagros collision zone along Ahvaz–Isfahan route in Iran. *Journal of Applied Geophysics*, **123**:112-122. http://dx.doi.org/10.1016/j.jappgeo.2015.10.001

Ostrovskiy E.Y. 1975. Antagonism of Radioactive Elements in Wallrock Alterations Fields and its Use in Aerogamma Spectrometric Prospecting. *International Geology Review*, **17**(4):461-468. https://doi.org/10.1080/00206817509471687

Patra I., Srinivas D., Tripathi S., Patel A.K., Ramesh Babu V, Raju B.V.S.N., Chaturvedi A.K. 2016. High-resolution Airborne Gamma ray Spectrometric data in Geological mapping-A case study from parts of Shillong Basin, Meghalaya. *Journal of Geophysics*, **37(3)**:173-178. https://inis.iaea.org/search/search.aspx?orig_q=RN:47110784

Quadros T.F.P., Koppe J.C., Strieder A.J., Costa J.C.L.C. 2003. Gamma-Ray Data Processing and Integration for Lode-Au Deposits Exploration. *Natural Resources Research*, **12**(1):57-65. https://doi.org/10.1023/A:1022608505873

Ramos L.N.R.A., Pires A., Toledo C.L.B. 2014. Airborne gamma-ray spectrometric and magnetic signatures of Fazenda Nova Region, East portion of Arenópolis magmatic arc, Goiás. *Revista Brasileira de Geofísica*, **32**(1):123-140. http://dx.doi.org/10.22564/rbgf.v32i1.401

Ramsay J.G. 1980. The crack-seal mechanism of rock deformation. *Nature*, **284**:135-139. https://doi.org/10.1038/284135a0

Roest W.R., Verhoef J., Pilkington M. 1992. Magnetic interpretation using the 3-D analytic signal. *Geophysics*, **57**(1):116-125. https://doi.org/10.1190/1.1443174

Santos E.J. 1995. *O complexo granítico Lagoa das Pedras: acresção e colisão na região de Floresta (Pernambuco), Província Borborema*. PhD Thesis, Instituto de Geociências da Universidade de São Paulo, São Paulo, p. 228.

Santos E.J. 1996. Ensaio preliminar sobre terrenos e tectônica acrescionária na Província Borborema. *In*: Congresso Brasileiro de Geologia, 39., Salvador. *Proceedings*... Salvador: SBG, p. 47-50.

Santos E.J., Brito Neves B.B., Van Schmus W.R., Oliveira R.G., Medeiros V.C. 2000. An overall view on the displaced terrane arrangement of the Borborema Province, NE Brazil. *In*: International Geological Congress, 31th, General Symposia, Tectonic Evolution of South American Platform. *Proceedings*... Rio de Janeiro, Brazil, p. 5-9.

Santos E.J. & Medeiros V.C. 1999. Constraints from granitic plutonism on Proterozoic crustal growth of the transverse zone, Borborema province, NE-Brazil. *Revista Brasileira de Geociências*, **29**(1):73-84. https://doi.org/10.25249/0375-7536.1999297384

Santos E.J., Souza Neto J.A., Silva M.R.R., Beurlen H., Cavalcanti J.A.D., Silva M.G., Dias V.M., Costa A.F., Santos L.C.M.L., Santos R.B. 2014. Metalogênese das porções norte e central da Província Borborema. *In*: Silva M.G., Rocha Neto M.B., Jost H., Kuyumijan R.M. (Eds.), *Metalogênese das províncias tectônicas brasileiras*. Belo Horizonte: CPRM, p. 343-388.

Santos E.J., Van Schmus W.R., Kozuch M., Brito Neves B.B. 2010. The Cariris Velhos tectonic event in Northeast Brazil. *Journal of South American Earth Sciences*, **29**(1):61-76. https://doi.org/10.1016/j.jsames.2009.07.003

Santos L.C.M.L., Dantas E.L., Cawood P.A., Lages G.A., Lima H.M., Santos E.J. 2018. Accretion tectonics in western Gondwana deduced from Sm-Nd isotope mapping of terranes in the Borborema Province, NE Brazil. *Tectonics*, **37**(8):2727-2743. https://doi.org/10.1029/2018TC005130

Santos L.C.M.L., Dantas E.L., Cawood P.A., Santos E.J., Fuck R.A. 2017a. Neoarchean crustal growth and Paleoproterozoic reworking in the Borborema Province, NE Brazil: insights from geochemical and isotopic data of TTG and metagranitic rocks of the Alto Moxotó Terrane. *Journal of South American Earth Sciences*, **79**:342-363. https://doi.org/10.1016/j.jsames.2017.08.013

Santos L.C.M.L., Dantas E.L., Santos E.J., Santos R.V., Lima H.M. 2015. Early to late Paleoproterozoic magmatism in NE Brazil: the Alto Moxotó Terrane and its tectonic implications for the pre-Western Gondwana assembly. *Journal of South American Earth Sciences*, **58**:188-209. https://doi.org/10.1016/j.jsames.2014.07.006

Santos L.C.M.L., Dantas E.L., Vidotti R., Cawood P., Santos E., Fuck R., Lima H. 2017b. Two-stage terrane assembly in Western Gondwana: Insights from structural geology and geophysical data of central Borborema Province, NE Brazil. *Journal of Structural Geology*, **103**:167-184. https://doi.org/10.1016/j.jsg.2017.09.012

Scheid C. & Ferreira C.A. 1991. *Programa Levantamentos Geológicos Básicos do Brasil:* Estados de Pernambuco e Paraíba - Folha SB.24-Z-D-I-Patos. Escala 1:100.000. Carta Geológica, Carta Metalogenético-previsional. Texto explicativo. Brasília, DNPM/CPRM, 140 p.

Shives R.B.K., Charbonneau B.W., Ford K.L. 2000. The detection of potassic alteration by gamma-ray spectrometry-Recognition of alteration related to mineralization. *Geophysics*, **65**(6):2001-2011. https://doi.org/10.1190/1.1444884

Sial A. & Ferreira V. 2016. Magma associations in Ediacaran granitoids of the Cachoeirinha- Salgueiro and Alto Pajeú terranes, northeastern Brazil: Forty years of studies. *Journal of South American Earth Sciences*, **68**:113-133. https://doi.org/10.1016/j.jsames.2015.10.005

Silva Filho M.A. 1989. *Projeto Itapetim:* relatório final de pesquisa de ouro; DNPM 840280 e 286/85. Internal report. Recife, CPRM.

Souza Neto J., Legrand J., Volfinger M., Pascal M.-L., Sonnet P. 2008. W-Au skarns in the Neo-Proterozoic Seridó Mobile Belt, Borborema Province in northeastern Brazil: An overview with emphasis on the Bonfim deposit. *Mineralium Deposita*, **43**(2):185-205. https://doi.org/10.1007/s00126-007-0155-1

Suh C.E., Lehmann B., Mafany G.T. 2006. Geology and geochemical aspects of lode gold mineralization at Dimako- Mboscorro SE Cameroon. *Geochemistry: Exploration, Environment, Analysis*, **6**(4):295-309. https://doi.org/10.1144/1467-7873/06-110

Takodjou Wambo J.D., Ganno S., Djonthu Lahe Y.S., Kouankap Nono G.D., Fossi D.H., Tchouatcha M.S., Nzenti J.P. 2018. Geostatistical and GIS analysis of the spatial variability of alluvial gold content in Ngoura-Colomines area, Eastern Cameroon: Implications for the exploration of primary gold deposit. *Journal of African Earth Sciences*, **142**:138-157. https://doi.org/10.1016/j.jafrearsci.2018.03.015

Van Schmus W.R., Brito Neves B.B., Hackspacher P.C., Babinski M. 1995. U/Pb and Sm/Nd geochronologic studies of the eastern Borborema Province, Northeast Brazil: initial conclusions. *Journal of South American Earth Sciences*, **8**(3-4):267-288. https://doi.org/10.1016/0895-9811(95)00013-6

Van Schmus W.R., Kozuch M., Brito Neves B.B. 2011. Precambrian history of the Zona Trasnversal of the Borborema Province, NE Brazil; Insights from Sm-Nd and U-Pb geochronology. *Journal of South American Earth Sciences*, **31**(2-3):227-252. https://doi.org/10.1016/j.jsames.2011.02.010

Van Schmus W.R., Oliveira E.P., Silva Filho A.F., Toteu F., Penaye J., Guimarães I.P. 2008. Proterozoic links between the Borborema province, NE Brazil, and the central African fold belt. *Geolical Society of London*, **294**(1):66-69. https://doi.org/10.1144/SP294.5

Wanderley A.A. 1999. *Projeto Itapetim*. Relatório Final de Pesquisa (alvarás: 721, 280, 281, 283/96). Internal report. Brasil, Serviço Geológico Braileiro (CPRM), 24 p.

Wemegah D., Preko K., Noye R., Boadi B., Menyeh A., Danuor S., Amenyoh T. 2015. Geophysical Interpretation of Possible Gold Mineralization Zones in Kyerano, South-Western Ghana Using Aeromagnetic and Radiometric Datasets. *Journal of Geoscience and Environment Protection*, **3**(4):67-82. http://dx.doi.org/10.4236/gep.2015.34008

Whitney D.L. & Evans B.W. 2010. Abbreviations for names of rock-forming minerals. *American Mineralogist*, **95**(1):185-187. https://doi.org/10.2138/am.2010.3371